Effects of three-body (Axilrod-Teller) forces on the classical and quantum behavior of rare-gas trimers

Charusita Chakravarty
Department of Chemistry, Indian Institute of Technology-Delhi, Hauz Khas, New Delhi 110016, India

Robert J. Hinde
Department of Chemistry, University of Tennessee, Knoxville, Tennessee 37996-1600

David M. Leitner
Department of Chemistry, University of Illinois, Urbana, Illinois, 61801

David J. Wales
University Chemical Laboratories, Lensfield Road, Cambridge CB2 1EW, United Kingdom

(Received 25 March 1997)

We have studied the structure and dynamics of nonrotating rare-gas trimers bound by a potential that combines two-body Lennard-Jones interactions and three-body Axilrod-Teller (triple dipole) interactions. Both classical and quantum trimers are examined. We investigate the onset and development of chaotic dynamics in the classical clusters by computing the Liapunov exponents associated with various phase space trajectories. In our studies of the quantum clusters, we examine the structure of the vibrational eigenstates, the statistical properties of the distribution of energy levels, and the average cluster structure at finite temperatures. Both avenues of research are principally aimed at understanding the effect of the three-body term on the clusters' behavior. We find that the three-body term gives rise to an integrable or nearly integrable component of phase space that is associated with the clusters' linear configuration and that manifests itself in both the classical and quantum properties of the trimers. The finite temperature structures predicted for quantum Ne_3 clusters suggest that over the range of parameters considered here, these clusters are sufficiently delocalized that properties associated with the linear configuration should be readily observable, even at very low temperatures. [S1063-651X(97)12107-9]

PACS number(s): 05.45.+b, 36.40.Sx, 34.20.Cf, 03.65.Ge

I. INTRODUCTION AND BACKGROUND

The structure and dynamics of weakly bound van der Waals molecules and clusters continue to be topics of active study in chemical physics, in part because of the relative ease with which such species can be investigated both experimentally and theoretically, and in part because of the wide range of chemical and physical phenomena that can be better understood through such studies. These phenomena include the nature of intermolecular forces, the onset of bulk thermodynamic behavior as a function of cluster size, the effect of three-body and many-body forces on the structure and dynamics of nonrigid molecules, and vibrational chaos in weakly bound systems. References [1] and [2] contain ''snapshots'' of recent research on van der Waals complexes.

Some of the most thoroughly studied van der Waals systems are homogeneous clusters of rare-gas atoms. Theoretical investigations of rare-gas clusters are particularly attractive because these systems serve as benchmarks for studying the effects of quantum mechanical behavior in weakly bound systems. Rare-gas clusters from He_n to Xe_n are bound together by interatomic forces that are qualitatively and quantitatively very similar when expressed in reduced units. Hence variations in the structure and dynamics of these clusters can be largely attributed to quantum mechanical effects arising from the wide range of atomic masses represented in the last column of the Periodic Table. For example, He_n clusters are often cited as prototypical quantum clusters [3,4], while the much heavier Xe_n clusters should behave essentially classically. Furthermore, the importance of quantum statistics in van der Waals systems is readily explored by comparing the behavior of ^3He_n and ^4He_n clusters [5].

In this paper we investigate the structural and dynamical changes in the homogeneous rare-gas trimers Ne_3, Ar_3, Kr_3, and Xe_3, which result from the addition of a strong three-body Axilrod-Teller (AT) term to the conventional two-body Lennard-Jones (LJ) cluster binding potential. Both classical and quantum mechanical properties of the clusters are studied. The strength of the AT potential term is determined by a single adjustable parameter, which may be varied to generate a family of very different potential energy surfaces. The combined Lennard-Jones-Axilrod-Teller (LJAT) potential thus presents us with a model system in which to explore how classical and quantum properties of van der Waals clusters are influenced by the topography of the underlying potential energy surface (PES).

We note that Horn *et al.* [6] have undertaken quantum mechanical studies of the low-lying vibrational states of Ar_3 clusters using two- and three-body potential energy terms that are substantially more realistic than the LJAT potential we study here. Our aims, however, are quite different from those of Horn *et al.*, who emphasize the need for spectroscopic accuracy and state-by-state assignment of the vibrational eigenstates. We are primarily concerned with un-

TABLE I. Lennard-Jones parameters used in this work. The quantum parameter $\eta=\hbar/\sigma\sqrt{m\epsilon}$ is also given.

	σ (Å)	ϵ (cm^{-1})	m (amu)	η
Ne	2.749	25.0	20.18	0.0945
Ar	3.405	84.0	39.948	0.0294
Kr	3.827	115.4	83.80	0.0155
Xe	4.100	156.4	131.30	0.0099

derstanding the relationship between the shape of the PES and the classical and quantum properties of rare-gas trimers. The combined LJAT potential is ideal for these purposes because of the control it gives us over the topography of the PES.

We begin by reviewing some theoretical and computational aspects of our work in Secs. II and III; we then present results for the classical and quantum LJAT trimers in Secs. IV and V, respectively. Throughout, we compare our results with earlier findings for trimers bound by LJ forces only. The results presented here suggest that the phase space of LJAT trimers is of a mixed nature, with both chaotic and regular components. We conclude with a brief discussion of the implications of this observation in Sec. VI.

II. THEORETICAL CONSIDERATIONS

A. Classical trimers

The classical Hamiltonian for LJAT trimers with atomic mass m is

$$H=\frac{1}{2m}\sum_{i=1}^{3}\mathbf{p}_i^2+4\epsilon\sum_{i<j=1}^{3}[(\sigma/r_{ij})^{12}-(\sigma/r_{ij})^{6}]+Z\sigma^9\epsilon\left[\frac{1+3\cos\theta_1\cos\theta_2\cos\theta_3}{(r_{12}r_{13}r_{23})^3}\right]. \quad (1)$$

The familiar two-body Lennard-Jones interaction is described by the energy and length scale parameters ϵ and σ; the dimensionless parameter Z determines the strength of the three-body Axilrod-Teller interaction, which depends on the cluster's three internal angles θ_1, θ_2, and θ_3. The form of the AT potential is such that for $Z>0$ it stabilizes near-linear configurations of the cluster and destabilizes the equilateral triangle and nearby configurations [7]. The LJ parameters we use in the current work are listed in Table I.

We characterize the dynamics of classical LJAT trimers by computing the Liapunov exponents along constant-energy molecular dynamics trajectories generated by Eq. (1). Liapunov exponents quantify the average long-time exponential rate of divergence of nearby trajectories in phase space. For an isolated triatomic system, there are only two Liapunov exponents that may be positive [8]; we denote these exponents as λ_1 and λ_2. If at least one of these exponents is positive, the system is chaotic; if both exponents are zero, the system is quasiperiodic. The sum of the positive exponents is the Kolmogorov entropy (K entropy), which measures the rate at which information about the state of the system is lost [9].

B. Quantum trimers

A dimensionless quantum mechanical Hamiltonian can be obtained from Eq. (1) by defining the parameter $\eta=\hbar/\sigma\sqrt{m\epsilon}$:

$$\hat{H}=-\frac{\eta^2}{2}\sum_{i=1}^{3}\nabla_i^2+V(q_{12},q_{23},q_{13};Z)/\epsilon, \quad (2)$$

where V is the LJAT potential presented above, and the dimensionless coordinates $q_{ij}=r_{ij}/\sigma$. The eigenstates of the quantum Hamiltonian are fully parametrized by η and Z; the η values for the trimers considered here are listed in Table I. The classical limit is approached as $\eta\to 0$.

We obtain the vibrational energy levels for the trimers using the discrete variable representation (DVR) approach outlined below in Sec. III, and examine various statistical properties of the level distributions. The statistical measures we concentrate on here are $P(S)$, the distribution of spacings between successive energy levels, and $\Delta_3(L)$, the mean spectral rigidity over a range L of energy levels. Reference [10] contains detailed definitions of the $P(S)$ and $\Delta_3(L)$ statistics, along with an extensive review of the relevant statistical properties of spectra. Here we simply note that $P(S)$ and $\Delta_3(L)$ are complementary statistical descriptions of the level spectrum of a system; $P(S)$ quantifies the short-range correlations between successive energy levels, while $\Delta_3(L)$ measures, over a large energy range L, the least squares deviation of the total sum of states from a straight line fit.

The spectral statistics obtained from quantum Hamiltonians with chaotic classical analogs have been found to obey predictions based on random matrix theory (RMT) [10]. A very good approximation to the RMT prediction for $P(S)$ is the Wigner distribution

$$P_{\mathrm{W}}(S)=\frac{\pi S}{2}\exp(-\pi S^2/4). \quad (3)$$

The RMT prediction for the spectral rigidity in the large L limit is

$$\Delta_{3,\mathrm{RMT}}(L)=\frac{\ln L}{\pi^2}-0.007. \quad (4)$$

Both of these predictions are for a range of energy levels that have been ''unfolded'' to obtain a spectrum with unit mean level density.

Quantum Hamiltonians whose classical analogs are integrable are found to obey Poisson statistics [10]. In this case, the distribution of spacings between successive energy levels is

$$P_{\mathrm{P}}(S)=e^{-S} \quad (5)$$

and the spectral rigidity is

$$\Delta_{3,\mathrm{P}}(L)=L/15. \quad (6)$$

Systems may display statistical properties that are intermediate between the chaotic (RMT) and integrable (Poisson) limits. This corresponds to the coexistence of regular and irregular regions in the phase space of the classical Hamil-

tonian. This behavior can be understood as a superposition of properly weighted contributions from RMT-type and Poisson-type quantum statistics, which arise, respectively, from chaotic and integrable components of phase space in the analogous classical Hamiltonian. For the simplest case of two disjoint components of classical phase space, one with relative weight q, which is chaotic, and one with weight $(1-q)$, which is regular, Berry and Robnik [11] have derived a formula for $P(S)$ that interpolates between the RMT and Poisson limits presented above:

$$P(S;q)=(1-q)^2\mathrm{erfc}(\sqrt{\pi}qS/2)\exp[-(1-q)S] +[2q(1-q)+\pi q^3 S/2] \times\exp[-(1-q)S-\pi q^2 S^2/4]. \quad (7)$$

Pandey [12] has given an expression for the spectral rigidity Δ_3, which also interpolates between the regular and chaotic limits:

$$\Delta_3(L;q)=\Delta_{3,\mathrm{RMT}}(qL)+\Delta_{3,\mathrm{P}}((1-q)L). \quad (8)$$

The DVR calculations outlined in Sec. III yield the eigenstates of the quantum LJAT trimers and thereby give us some information about how the quantum trimers explore different regions of the PES. We are also interested in understanding how the quantum clusters sample the PES at various temperatures; here, we expect to see strong differences between the classical and quantum trimers, at least for sufficiently small atomic masses.

As an example, consider the $T=0$ limit. At $T=0$, the spatial distribution function for the classical trimers will simply be $\delta(\mathbf{x}-\mathbf{x}_{\min})$, where $\mathbf{x}$ represents all of the cluster's internal degrees of freedom, and $\mathbf{x}_{\min}$ specifies the location of the global minimum on the PES. The $T=0$ spatial distribution function for the quantum trimers will be given by the probability density $P(\mathbf{x})=|\Psi_0(\mathbf{x})|^2$ associated with the ground state wave function $\Psi_0(\mathbf{x})$. For small values of the atomic mass m, ground state tunneling and zero-point energy effects will lead to finite (nonzero) probabilities of observing configurations of the quantum cluster associated with higher energy minima, even at $T=0$. In the absence of fermionic antisymmetrization requirements, $\Psi_0(\mathbf{x})$ is nodeless. Configurations can be sampled from such a wave function using diffusion quantum Monte Carlo techniques (outlined below) so as to gauge the extent to which the wave function is localized in a particular minimum.

At nonzero temperatures, the spatial distribution function for the quantum cluster will be given by the diagonal density matrix element in the canonical ensemble, $P(\mathbf{x})=\langle\mathbf{x}|e^{-\beta H}|\mathbf{x}\rangle$, where $\beta=1/kT$. In the eigenfunction representation, we have

$$P(\mathbf{x})=\sum_n |\Psi_n(\mathbf{x})|^2 e^{-\beta E_n} \quad (9)$$

where $\{\Psi_n(\mathbf{x})\}$ are the eigenstates of the Hamiltonian with respective eigenvalues $\{E_n\}$. Finite temperature spatial distributions can be generated by path integral Monte Carlo methods. In this study, we use diffusion and path integral Monte Carlo techniques to compute the ground state wave function and the finite temperature spatial distribution functions for the quantum LJAT trimer Ne_3. These quantum Monte Carlo techniques are described briefly below.

III. COMPUTATIONAL METHODS

A. Liapunov exponents

The techniques we use to compute the Liapunov exponents of the classical LJAT trimers have been described in detail elsewhere [13,14]. Briefly, we integrate numerically the equations of motion for finite length vectors that reside in the tangent space of the trimer; these equations of motion depend parametrically on a constant-energy reference trajectory that the trimer follows in phase space and that is generated by the Hamiltonian given in Eq. (1). We periodically compute the Liapunov exponents by measuring the extent by which the tangent space vectors have grown or shrunk since the trajectory's beginning.

In the present study, we integrate the reference trajectory and the tangent space equations of motion for 10^5 time steps of length 10^{-14} s each. After every 1000 steps, we compute the Liapunov exponents based on the lengths of the tangent space vectors; we then take the final set of exponents obtained at the end of the trajectory as our estimates of the true exponents.

Strictly speaking, Liapunov exponents are only defined in the limit $t\rightarrow\infty$, and the exponents we calculate are properly called ''finite-time'' Liapunov exponents. One way to assess how closely our computed exponents approximate the true $t\rightarrow\infty$ exponents is to compare the results obtained from different trajectories. This is because for ergodic systems, the $t\rightarrow\infty$ Liapunov exponents are independent of the initial conditions [8]. We therefore compute 100 trajectories at each energy and consider the distribution of exponents after 10^5 steps. The initial conditions for the batches of 100 trajectories are drawn from a microcanonical ensemble [15,16] with total angular momentum $J=0$.

If a batch of 100 trajectories gives a relatively narrow distribution of Liapunov exponents after 10^5 steps, it seems likely that the finite-time exponents are close approximations to the $t\rightarrow\infty$ exponents. If, however, the trajectories generate a wide distribution of final exponents, we know that either longer trajectories are required or the phase space sampled by the trajectories is not a single ergodic component.

B. Vibrational eigenstates

To compute the vibrational energy levels and eigenstates of the $(J=0)$ quantum LJAT trimers, we use the three-dimensional DVR method with successive diagonalization and truncation, as developed by Whitnell, Light, and coworkers [17–19].

The Hamiltonian in Eq. (2) can be written as a function of three internal coordinates when only states with total angular momentum $J=0$ are considered. We express this three-dimensional Hamiltonian in terms of Pack's adiabatic principal axis hyperspherical (APH) coordinates [20,21] in order to exploit the symmetry of the trimers and thereby reduce the computational effort required to calculate the eigenfunctions.

Pack's APH coordinates (ρ,θ,χ) are defined in terms of the mass-scaled Jacobi coordinates (r,R,ϕ) for a three-atom

system. These mass-scaled coordinates depend on a dimensionless constant c, which is a function of the masses of the three atoms; when all three atoms have the same mass, $c=(3/4)^{1/4}$. In the mass-scaled Jacobi scheme, $c\mathbf{r}$ is the interatomic vector between two of the three atoms, $c^{-1}\mathbf{R}$ is the vector from the center of mass of these two atoms to the position of the third atom, and ϕ is the angle between $\mathbf{R}$ and $\mathbf{r}$.

With this definition of the mass-scaled Jacobi coordinates, and letting

$$S=\sqrt{(R^2-r^2)^2+(2Rr\cos\phi)^2}, \tag{10}$$

the APH coordinates are

$$\begin{aligned}\rho^2&=r^2+R^2,\\ \tan\theta/2&=S/(2Rr\sin\phi),\\ \sin2\chi&=(2Rr\cos\phi)/S,\\ \cos2\chi&=(R^2-r^2)/S.\end{aligned} \tag{11}$$

The limits of these APH coordinates are $0\leqslant\rho\leqslant\infty$, $0\leqslant\theta\leqslant\pi$, and $0\leqslant\chi<2\pi$. Linear configurations of the trimer correspond to $\theta=\pi$; the equilateral triangle configuration corresponds to $\theta=0$ (with all χ values being equivalent).

The finite basis representations used to generate the DVR in Pack's APH coordinates are the same as those used by Whitnell and Light [18,19] in their study of H_3^+. The DVR points for the ρ and χ coordinates are equally spaced, with those in χ covering the entire range $0\leqslant\chi<2\pi$. The DVR points for ρ span a specified and adjustable range in this coordinate. The DVR parameters used in the current calculations are quite similar to those used in earlier studies of LJ trimers [22], and we refer the reader to these studies for details.

The ground states of the trimers can also be computed using diffusion quantum Monte Carlo (DQMC) techniques. This approach is based on the fact that by introducing the imaginary time variable $\tau=it/\hbar$, we can write the time-dependent Schrödinger equation for the clusters as a diffusion equation

$$\frac{\partial\Psi}{\partial\tau}=\frac{\hbar^2}{2m}\sum_{i=1}^{3}\nabla_i^2\Psi-V\Psi, \tag{12}$$

where $\hbar^2/2m$ is the diffusion constant and $V\Psi$ represents a first-order forcing term. As $\tau\rightarrow\infty$, the solution to Eq. (12) approaches asymptotically the trimer's ground state wave function Ψ_0. A set of configurations $\{\mathbf{x}\}$ distributed with probability $\Psi_0(\mathbf{x})$ can be generated from this wave function using a simple unbiased DQMC procedure, which computes the asymptotic solution to Eq. (12) by following the diffusive motion of ''replicas'' in configuration space using random walk techniques [23–27]. In such a DQMC simulation, all replicas have equal weight; reweighting must be done in order to generate the distribution corresponding to $|\Psi_0|^2$. Such reweighting procedures are relatively elaborate and computationally expensive, and are therefore not pursued here.

In our DQMC scheme, the wave function is represented by a distribution of 1000 replicas. The replicas are propagated iteratively using the short-time propagator (expressed in atomic units)

$$\begin{aligned}P(\mathbf{x}_{n+1},\mathbf{x}_n)=&\exp\{-\Delta t[V(\mathbf{x}_{n+1})-E]\}\sqrt{m/2\pi\Delta t}\\ &\times\exp[-m(\mathbf{x}_{n+1}-\mathbf{x}_n)^2/2\Delta t],\end{aligned} \tag{13}$$

where Δt is the time step.

For the Ne_3 cluster, we used a time step of $\Delta t=100$ atomic units, and propagated the replicas for 5×10^4 to 1×10^5 time steps to obtain ground state energies that were converged to better than 1% (as compared with the DVR calculations). Once the energy had converged, we propagated the replicas for another 10^5 time steps; after every 10^4 steps, we performed a steepest descent quench on each replica to measure the fraction of replicas occupying the triangular basin, $f_{\rm tri}$, and the fraction occupying the linear basin, $f_{\rm lin}=1-f_{\rm tri}$. The occupancies calculated from these 10 quenches were then averaged. While $f_{\rm tri}$ and $f_{\rm lin}$ will not be exactly the same as the ground state occupancies of the two minima, because the replicas are distributed according to Ψ_0 and not $|\Psi_0|^2$, there is evidence from the results of our study that for Ne_3 the two sets of quantities are not very different. In view of the fact that if Ψ_0 is largely localized in a given basin, $|\Psi_0|^2$ will also be, this is not surprising.

C. Finite temperature quantum properties

The finite temperature properties of the quantum LJAT Ne_3 cluster are computed using the Fourier path integral Monte Carlo (PIMC) technique [28–32]. In this method, a Metropolis Monte Carlo simulation is used to sample the coordinate space variables $\mathbf{x}$ and the Fourier coefficients $\mathbf{a}$, which represent the various quantum paths of the system. The Metropolis weight function for this Monte Carlo simulation is

$$W(\mathbf{x},\mathbf{a})=\exp\left[-\beta\langle V_{\rm eff}\rangle-\sum_n\frac{\mathbf{a}_n^2}{2\sigma_n^2}\right] \tag{14}$$

where $\beta=1/kT$, $\sigma_n^2=2\beta\hbar^2/m\pi^2n^2$, and $\langle V_{\rm eff}\rangle$ is the partially averaged potential associated with the quantum path. A PIMC simulation will generate a set of configurations $\{\mathbf{x}\}$ distributed according to their probability of occurrence, $P(\mathbf{x})$, in the canonical ensemble [see Eq. (9)]. A steepest descent quench can be performed for each sampled configuration to test whether it lies in the triangular or linear basin, as in the DQMC simulations. For more details on the PIMC method and on the definition of $\langle V_{\rm eff}\rangle$, the reader should see the references listed above. In our calculations, 16 Fourier coefficients $\{\mathbf{a}_n\}$ are used per degree of freedom per particle. Each PIMC run consists of 2.5×10^6 configurations, of which 500 were quenched as described above to determine $P_{\rm tri}$ and $P_{\rm lin}$.

For comparison with the quantum results, classical spatial probability distributions were obtained at finite temperatures $T>0$ for the LJAT Ne_3 cluster using standard Metropolis Monte Carlo procedures. At each value of Z, 5×10^5 configurations were generated, with an acceptance ratio of roughly 50%. Five hundred of these configurations were

sampled (at intervals of 1000 MC steps) and were quenched to determine the relative classical occupancies of the triangular and linear minima on the PES.

Estimated statistical errors for both the classical and quantum occupancies were obtained at selected values of Z by binning and quenching 5000 configurations (instead of 500) and calculating the triangular and linear occupancies for ten blocks of 500 configurations.

IV. RESULTS AND DISCUSSION: CLASSICAL TRIMERS

A. Potential surface topography

In the absence of the three-body AT term, the PES of the LJ trimer has a single global minimum corresponding to the equilateral triangle D_{3h} geometry. By adding the three-body term to the potential, we introduce a new parameter Z that we may vary continuously to modify the topography of the PES. For $Z>0$ the AT term stabilizes near-linear configurations of the cluster and destabilizes the equilateral triangle [7]. For $Z \geqslant 0.4$ the AT potential is strong enough that the linear $D_{\infty h}$ configuration, which is a saddle point for $Z=0$, becomes a local minimum. This new local minimum is higher in energy than the D_{3h} global minimum, and is separated from it by a ''bent'' transition state corresponding to an obtuse C_{2v} isosceles triangle. As Z increases, the linear minimum becomes deeper and the D_{3h} minimum becomes shallower, until at $Z \geqslant 1.8$ the linear structure becomes the new global minimum.

Figure 1 depicts the reaction path for rearrangement between the two minima at selected Z values. Note that at lower Z values, the isomerization coordinate (which corresponds essentially to the bending normal mode of the C_{2v} transition state) exhibits much greater negative curvature as the cluster descends into the triangular minimum than it does for descent into the linear minimum.

B. Liapunov exponents

Figure 2(a) shows the distribution of final K-entropy values $K=\lambda_1+\lambda_2$ obtained from a batch of 100 trajectories for the Ar_3 trimer with $Z=1$ at $E=-1.69\epsilon$. Each trajectory represented in this figure begins from initial conditions for which a steepest descent quench leads to the D_{3h} minimum. For comparison, Fig. 2(b) shows the distribution of final K entropies obtained from a batch of 100 trajectories for the same cluster at the same energy, but using trajectories that are initiated from coordinates for which quenching leads to the linear minimum. The regions of configuration space for which quenches lead to particular stationary points are the ''basins of attraction'' of these structures. Such basins have previously been visualized for triatomic systems in a different context [33,34] and feature in a new global optimization algorithm described elsewhere [35].

We see immediately that there are significant differences between the two batches of trajectories. Those trajectories beginning in the triangular basin give rise to a unimodal distribution of K-entropy values peaked around $K \approx 1.1$ bits/ps. The K-entropy distribution for the trajectories initiated in the linear basin, however, is distinctly trimodal, with peaks at $K \approx 0$, 0.2, and 1.1 bits/ps.

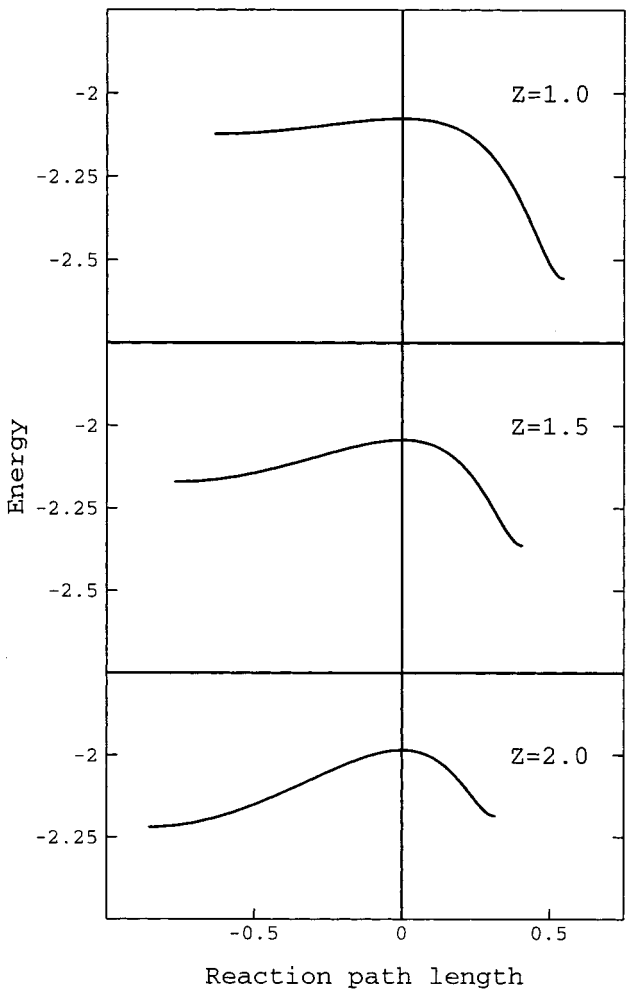

FIG. 1. Reaction paths for the LJAT trimers with (a) $Z=1$, (b) $Z=1.5$, and (c) $Z=2$. The energy along the reaction path is plotted in units of the LJ parameter ϵ; progress along the reaction path (x) is measured in units of $\sigma\sqrt{m}$, where m and σ are the LJ parameters given in Table I. The saddle point is at $x=0$; positive x values correspond to the triangular basin and negative x values correspond to the linear basin. The energy of the saddle point is -2.076ϵ, -2.043ϵ, and -1.985ϵ for $Z=1$, 1.5, and 2, respectively.

The multimodal nature of the K-entropy distribution shown in Fig. 2(b) suggests that the batch of trajectories initiated from within the linear basin does not sample a single, ergodic component of phase space. Further evidence for this hypothesis comes from a closer examination of the trajectories themselves. We find that several of these trajectories remain in the linear basin for the entire span of 10^5 time steps, despite the fact that at $E=-1.81\epsilon$, the cluster has enough energy to escape from this region (as seen from Fig. 1). These ''trapped'' trajectories are responsible for the two peaks shown in Fig. 2(b) at low values of K.

In contrast, the trajectories that begin in the linear basin but ultimately cross over the saddle separating the two minima have K-entropy values that are similar to those for the trajectories, which begin in the triangular basin, and which are clustered around $K \approx 1.1$ bits/ps. The trajectories that do cross the saddle, whether they begin in the linear or the triangular basin, make a few dozen (typically 40–60) passes across the saddle during the 10^5-step trajectory.

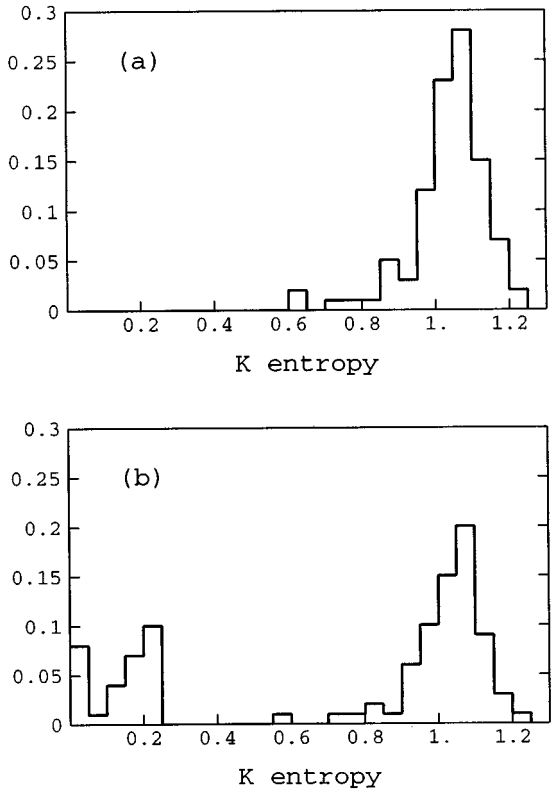

FIG. 2. Distribution of final K-entropy values $K=\lambda_1+\lambda_2$ for $Z=1$ LJAT Ar_3 at $E=-1.69\epsilon$. (a) Distributions for 100 trajectories initiated in the triangular basin. (b) Distributions for 100 trajectories initiated in the linear basin. The K entropy is given in units of bits/ps.

We next look more closely at the low K-entropy portion of Fig. 2(b) to determine whether the apparent bimodality of this part distribution is real or an artifact. We do this by computing final Liapunov exponents for a larger set of trajectories (168 in all) at $E=-1.69\epsilon$, which begin in the linear basin and remain there for 10^5 time steps. The distribution of K values thereby obtained is shown in Fig. 3. From these results, it appears that the peak located at $K\approx 0.2$ bits/ps is genuine.

The results presented in Figs. 2 and 3 suggest that the $Z=1$ LJAT Ar_3 cluster has three main regions of phase

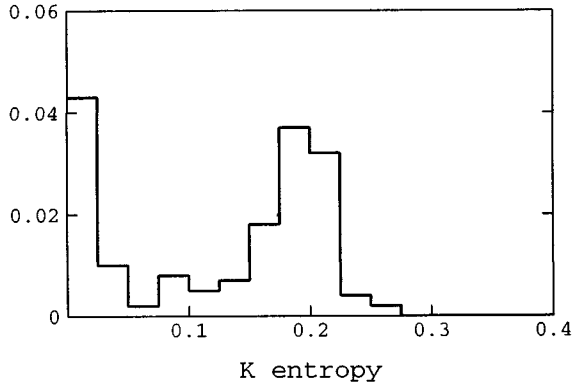

FIG. 3. Distribution of final K-entropy values for $Z=1$ LJAT Ar_3 at $E=-1.69\epsilon$ for a set of 168 trajectories that begin in the linear basin and remain trapped there for 10^5 time steps. The K entropy is given in units of bits/ps.

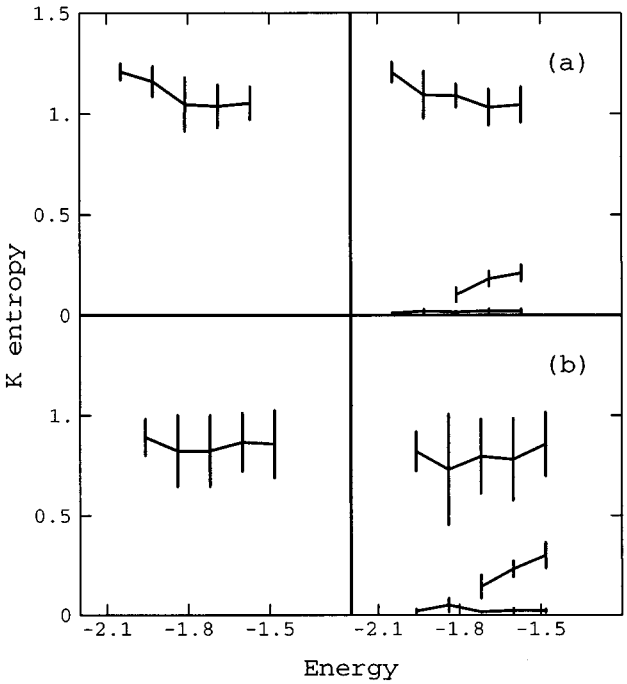

FIG. 4. K-entropy values representative of the various components of phase space in LJAT Ar_3 at (a) $Z=1$ and (b) $Z=2$. The left panel of each figure shows the K entropy for the strongly chaotic trajectories initiated in the triangular basin. The right panel of each figure shows the K-entropy values for the two or three regions of phase space sampled by trajectories initiated in the linear basin. Error bars extend one standard deviation in each direction. Lines have been drawn to guide the eye and have no physical significance. The K entropies are given in units of bits/ps and the energy in units of ϵ.

space at $E=-1.69\epsilon$. These are (1) a strongly chaotic ($K\approx 1.1$ bits/ps) region of phase space that spans both configurational basins and in which trajectories rapidly move between these basins; (2) a weakly chaotic ($K\approx 0.2$ bits/ps) region of phase space associated with trajectories that remain trapped in the linear basin for at least 10^5 time steps (or 1 ns); and (3) an essentially quasiperiodic region of phase space also associated with trajectories that remain trapped in the linear basin for 10^5 time steps or more. Broadly similar results are obtained for $Z=1$ Ar_3 at other energies, and for the $Z=2$ Ar_3 cluster and the $Z=0.5$ and $Z=1.5$ Xe_3 clusters across a range of energies, as shown in Figs. 4 and 5.

To produce these figures, we have calculated the K entropy $K=\lambda_1+\lambda_2$ for a batch of trajectories and examined probability distributions for K similar to those shown in Fig. 2. The ''end points'' of the peaks in these K distributions are determined by locating the local minima in the derivative of the cumulative probability distribution for K. Then an average K value and standard deviation for each peak is computed from those trajectories that make up that peak. Figures 4 and 5 show the average K values obtained in this fashion.

In each case we begin with a sample of 100 trajectories initiated in either the triangular or linear basin. The trajectories that begin in the triangular basin always produce a unimodal distribution of K values. At high energies, we find three peaks in the K-entropy distribution for trajectories that begin in the linear basin: one at large positive K values, one

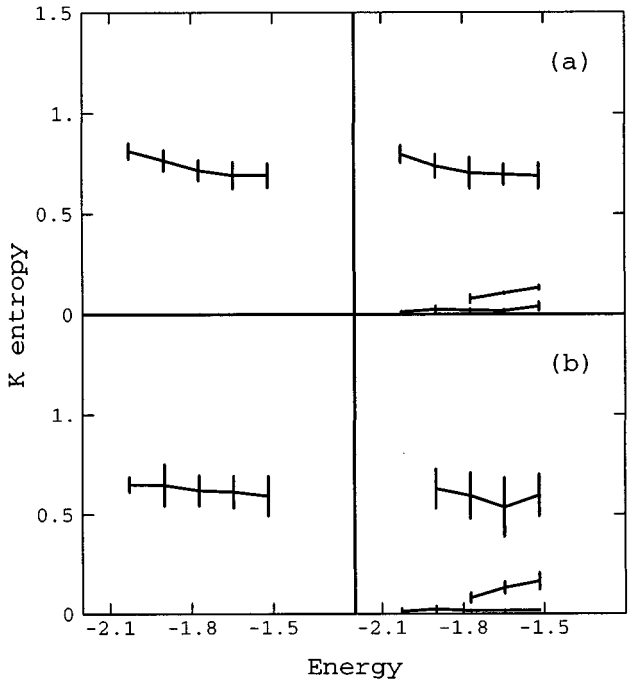

FIG. 5. K-entropy values representative of the various components of phase space in LJAT Xe_3 at (a) $Z=0.5$ and (b) $Z=1.5$. See the caption for Fig. 4 for further details.

at small positive K values, and one near zero. At lower energies, however, we typically observe only two peaks for these trajectories: one at large K values and one at nearly zero K values. The peaks with large K values are associated with trajectories that cross over the C_{2v} saddle point separating the basins on the PES, while the peaks with small K values are associated with trajectories that remain trapped in the linear basin. Each peak is represented by a single point in Figs. 4 and 5.

For three of the trimers—$Z=1$ and $Z=2$ Ar_3, and $Z=1.5$ Xe_3—at those energies where three K-entropy peaks are observed for trajectories initiated in the linear basin, we have examined a larger sample of 1000 trajectories beginning in this basin. Using only those trajectories in this sample that remain trapped in the linear basin for 10^5 time steps (typically 10% to 40% of the sample), we recompute K values for the weakly chaotic and quasiperiodic regions of phase space.

For comparison with the quantum results presented below, we have estimated the fraction of phase space associated with the various regions of phase space represented in Figs. 4 and 5. These calculations are performed as follows. We first estimate the relative weight of the triangular and linear basins (denoted $W_{\rm tri}$ and $W_{\rm lin}$) at each energy from a microcanonical sample [15,16] of 10^4 configurations. From the binning procedure just described, we can estimate the fraction of trajectories that, when initiated in the linear basin, fall into the weakly chaotic and essentially quasiperiodic regions of phase space. Let $W_{\rm wc,lin}$ and $W_{\rm qp,lin}$ denote these fractions. (At energies where no weakly chaotic portion of phase space is observed, we set $W_{\rm wc,lin}=0$.)

The relative sizes of the three regions of phase space—the strongly chaotic region that spans both basins (with weight $W_{\rm sc}$), the weakly chaotic region associated with the linear basin (with weight $W_{\rm wc}$), and the nearly quasiperiodic region associated with the linear basin (with weight $W_{\rm qp}$)—are then computed as follows:

$$W_{\rm qp}=W_{\rm lin}W_{\rm qp,lin}\,,$$

$$W_{\rm wc}=W_{\rm lin}W_{\rm wc,lin}\,, \tag{15}$$

$$W_{\rm sc}=1-W_{\rm qp}-W_{\rm wc}\,.$$

The results are summarized in Table II. They show that for $Z\geqslant 1$, the quasiperiodic and weakly chaotic regions occupy a substantial fraction of the entire phase space of the LJAT trimers. Although these two regions of phase space decline somewhat in importance as the energy increases, we see that even for energies well above the saddle point some 5–10% of the total phase space of the $Z\geqslant 1$ trimers is quasiperiodic or only weakly chaotic. In Sec. V we will show that similar behavior is observed in the quantum clusters.

C. Phase space structure

The LJAT trimers have three vibrational degrees of freedom (DOF). The phase space structure of Hamiltonian systems with three or more DOF is still incompletely understood. It is clear that in any system with mixed phase space, the regular (or quasiperiodic) and chaotic regions of phase space must be disjoint; what is not clear is whether the chaotic region of phase space can be further subdivided. Wiggins [36] showed that geometrical structures *may* exist in the phase space of three-DOF systems, which divide the phase space into disjoint regions separated by partial (or ''porous'') barriers. In a study of the three-DOF $He–I_2$ van der Waals complex which used a physically reasonable Hamiltonian, however, Gillilan and Ezra [37] could not locate these structures.

TABLE II. Relative weight of the quasiperiodic and weakly chaotic components of phase space in LJAT trimers. The error arising from the finite size of our trajectory batches is estimated to be ± 0.03.

$Z=0.5$ Xe_3			$Z=1$ Ar_3			$Z=1.5$ Xe_3			$Z=2$ Ar_3		
E (ϵ)	$W_{\rm qp}$	$W_{\rm wc}$	E (ϵ)	$W_{\rm qp}$	$W_{\rm wc}$	E (ϵ)	$W_{\rm qp}$	$W_{\rm wc}$	E (ϵ)	$W_{\rm qp}$	$W_{\rm wc}$
−2.028	0.01	0.0	−2.047	0.05	0.0	−2.028	0.33	0.0	−1.958	0.77	0.0
−1.900	0.01	0.0	−1.929	0.11	0.0	−1.900	0.33	0.0	−1.839	0.54	0.0
−1.772	0.01	0.01	−1.810	0.04	0.06	−1.772	0.08	0.16	−1.720	0.05	0.29
−1.645	0.01	0.01	−1.690	0.02	0.05	−1.645	0.03	0.16	−1.601	0.04	0.18
−1.517	0.01	0.01	−1.571	0.01	0.04	−1.517	0.01	0.08	−1.482	0.02	0.08

The results in Figs. 4 and 5 and in Table II indicate that the regions of phase space we have termed ''weakly chaotic'' and ''strongly chaotic'' are separated by some kind of barrier. Indirect evidence suggests that the barrier is porous. Note that the high-K peaks shown in Fig. 2 are relatively broad and are skewed toward lower K values. The trajectories that are responsible for this skewing are those that explore both the triangular and linear basins on the PES, but which at some point enter the linear basin and remain there for a substantial period of time. This indicates that transport between the weakly and strongly chaotic regions of phase space is possible. Nevertheless, the barrier between these regions is fairly effective at separating weakly chaotic behavior from strongly chaotic behavior, because a large number of weakly chaotic trajectories remain trapped in the linear basin for as long as 1 ns.

Inspection of the trapped trajectories shows that they are undergoing predominantly bending motion localized around the linear minimum energy geometry. The behavior of these trajectories is thus qualitatively similar to that of the stable ''horseshoe'' periodic orbit, which has been observed in several studies of H_3^+ [38–40]. We hypothesize that an analogous stable periodic orbit exists in the LJAT trimers for $Z \geqslant 1$, and that it is surrounded by a quasiperiodic ''sheath'' in phase space. The region of phase space we have identified as weakly chaotic is likely to be located just outside this sheath, and is separated from the remaining strongly chaotic portion of phase space by a partial barrier or phase space bottleneck. Trajectories that are initiated inside this weakly chaotic region of phase space, or which enter it from the strongly chaotic region, remain trapped for long periods of time because the interface between the weakly chaotic and quasiperiodic regions of phase space is ''sticky'' [41].

Yurtsever and Elmacı [42] have recently studied the chaotic dynamics of LJAT trimers with LJ parameters and atomic masses chosen to represent C_3 clusters. After an appropriate rescaling of the time variable t [43], their results can be compared where they overlap with ours, at $Z=0.5$ and $Z=1$. The relevant findings of Yurtsever and Elmacı (YE) are as follows: (1) in the range $0 \leqslant Z \leqslant 1$, high-energy ($E \geqslant -1.95\epsilon$) trajectories are strongly chaotic, whether they are initiated in the linear basin or in the triangular basin; and (2) in the intermediate Z range $0.25 \leqslant Z \leqslant 0.75$, low-energy ($E < -1.95\epsilon$) trajectories are weakly to moderately chaotic. Furthermore, in this range of Z and E, the degree of chaos exhibited by trajectories initiated in the linear basin increases as Z increases, while the degree of chaos exhibited by trajectories initiated in the triangular basin decreases as Z increases.

YE find that the long-time, low-energy behavior of their clusters depends strongly on the initial geometry; this lends support to the picture of the phase space structure that we have outlined above. At high energies, though, YE observe only strongly chaotic dynamics, in apparent disagreement with our qualitative picture. This discrepancy can be partially reconciled by considering the characteristic time scales for motion in YE's C_3 clusters and our rare-gas trimers. The classical trajectories computed by YE and by us are similar in duration (roughly 1 ns); however, the vibrational frequencies of C_3 clusters are much higher than those of rare-gas trimers. Therefore the C_3 trajectories are much longer in a *relative* sense, and it is plausible that YE's trajectories have escaped the ''sticky,'' weakly chaotic region of phase space and more closely represent the $t \to \infty$ Liapunov exponents of the LJAT system.

Finally, we note that our results, and those obtained by YE, can be rationalized in terms of a model based on the degree of negative curvature of the PES [44,45]. As Fig. 1 shows, the basin associated with near-linear configurations of the LJAT trimers exhibits relatively weak negative curvature near the saddle point, while the triangular basin is strongly negatively curved near the saddle. We have previously observed [44,45] a strong correlation between the degree of negative curvature on the PES and the magnitude of a system's local Liapunov exponents. This simple negative curvature model predicts that the triangular basin will give rise to more strongly chaotic behavior than will the linear basin, in agreement with our results. As Z increases, the degree of negative curvature in the linear basin increases, while that in the triangular basin decreases; this is in accord with YE's findings in the intermediate Z range.

V. RESULTS AND DISCUSSION: QUANTUM TRIMERS

The classical dynamical results presented in the previous section rest on the validity of the notion that the atoms in LJAT trimers follow well-defined trajectories in phase space. Such a viewpoint is ultimately incompatible with quantum mechanics, where the concept of a trajectory is absent. Hence it is important for us to consider the extent to which the classical picture presented above must be modified when quantum clusters are considered.

A. Quantum Monte Carlo calculations

We begin by assessing the role of zero-point effects in the vibrational ground state of the LJAT Ne_3 trimer, which has the largest η value of all the clusters studied here and which therefore is expected to show the most pronounced quantum phenomena. Using the DQMC techniques outlined above, we have computed as a function of Z the fraction of replicas representing the ground state that are located in the triangular and linear minima, $f_{\rm tri}$ and $f_{\rm lin}$, for the vibrational ground state of the Ne_3 cluster. Figure 6(a) shows how $f_{\rm tri}$ varies with Z for the Ne_3 cluster. The classical occupancies are also presented in this figure for easy comparison.

The point at which $f_{\rm tri}=0.5$ indicates a switchover from a predominantly triangular geometry (where $f_{\rm tri}>0.5$) to a predominantly linear geometry (where $f_{\rm tri}<0.5$). In the classical Ne_3 cluster, this switchover occurs at $Z \approx 1.8$, and can be understood in terms of the deepening of the linear minimum on the PES with increasing Z, as shown in Fig. 1. In the quantum cluster, the switchover occurs at $Z \approx 2.4$; the shift of the switchover point to higher Z values reflects the balance between the depths and the zero-point energies of the two minima.

Similar quantum delocalization effects are observed at finite temperatures. Figure 6(b) shows how $P_{\rm tri}$ varies with Z for the classical and quantum Ne_3 clusters at $T=2$ K. (Very similar results are obtained at $T=1$ and 1.5 K; for $T \geqslant 3$ K, though, the quantum cluster begins to evaporate, so the highest temperature used in the PIMC studies was $T=2$ K.) This figure indicates that the classical switchover occurs at

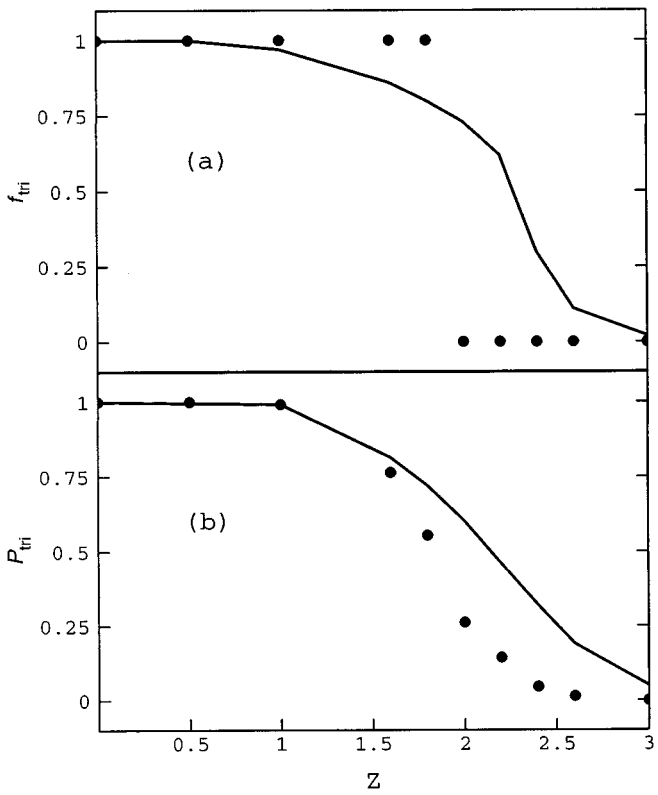

FIG. 6. (a) The Z dependence of f_{tri} for LJAT Ne_3, showing the degree of localization in the triangular minimum of the ground state wave function. (b) The Z dependence of P_{tri}, the relative occupancy of the triangular minimum, for LJAT Ne_3 at $T=2$ K. Estimated error bars are less than ± 0.04 for all values of Z. Points indicate the classical values of f_{tri} and P_{tri} for comparison.

$Z \approx 1.8$, and the quantum switchover at $Z \approx 2.3$. The difference between the quantum and classical switchover values indicates the importance of quantum effects at these temperatures. Moreover, the switchover values computed from f_{tri} at $T=0$ and from P_{tri} at $T=2$ K are very similar, indicating that ground state occupancies of the two minima must be close to f_{tri} and f_{lin}.

B. DVR calculations

The diffusion and path integral Monte Carlo results indicate that we must take quantum effects into account to properly describe the behavior of the Ne_3 LJAT trimer. Although we expect that the clusters with small η values will behave somewhat more classically, we have computed and examined vibrational eigenstates for all four of the trimers studied here, for comparison with both the classical trajectory results presented in Sec. IV and the quantum results obtained earlier [22,46,47] for trimers bound by LJ potentials alone. These calculations were performed using the DVR technique described above with Z values of 0.5, 1, and 1.5. At these values of Z, both the equilateral triangle and the linear configuration are minima on the PES; however, the former remains the global minimum throughout this range of Z values. This permits us to exploit the D_{3h} symmetry of the equilateral triangle in the DVR calculations. We note that for these trimers, which are all composed of bosons, only the A_1' levels are symmetry allowed in the $J=0$ vibrational manifold.

TABLE III. Ground state energies (in units of ϵ) of the quantum LJAT trimers for several Z values. Both DVR and DQMC results are given for Ne_3; only DVR results are given for the heavier clusters. The ground state configuration of each trimer is roughly an equilateral triangle; the classical energy of the D_{3h} global minimum on the potential surface is given for comparison.

Cluster	$Z=0$	$Z=0.5$	$Z=1$	$Z=1.5$
Ne_3 (DVR)	−1.718	−1.591	−1.479	−1.379
Ne_3 (DQMC)	−1.719	−1.585	−1.473	−1.374
Ar_3	−2.553	−2.358	−2.181	−2.020
Kr_3	−2.761	−2.548	−2.355	−2.179
Xe_3	−2.844	−2.626	−2.426	−2.235
Classical	−3.000	−2.757	−2.514	−2.271

Table III gives the energies of the vibrational ground states of the four trimers at these Z values. For comparison, the ground state energies computed by DQMC are also given, as are the energies of the global (triangular) minimum on the PES. We see that the quantum ground state energies are all higher than the classical minima; this difference is greatest for the Ne_3 cluster (which has the largest η value) and smallest for the Xe_3 cluster, which comes as no surprise. As Z increases, the quantum ground state energies for the heavier clusters approach the energies of the classical minima more closely. This can be understood qualitatively from the reaction paths presented in Fig. 1; the cluster's classical vibrational frequencies near the triangular minimum decrease as Z increases, and we expect that the magnitude of the zero-point energy will likewise decrease. We note, however, that the effect of increasing Z is rather modest for Ne_3. This suggests that as Z increases, the increasing occupancy of the higher-energy linear minimum in this cluster (as shown in Fig. 6) partially offsets the decrease of the vibrational frequencies at the triangular minimum because it tends to increase the potential energy.

This simple rationalization of the decrease in the zero-point energy with increasing Z raises the question of how closely the energy of the quantum ground states can be estimated using a normal mode approach. For the LJ Ar_3, Kr_3, and Xe_3 trimers, the energies of the vibrational ground states were found to be very close to those obtained, using a simple separable normal mode approximation, from the classical vibrational frequencies at the triangular minimum on the PES [22]. Table IV gives normal mode estimates for the ground state energies of the four LJAT trimers at various Z values. Note that the normal mode estimates are always higher than the actual ground state energies, and the agree-

TABLE IV. Normal mode estimates (in units of ϵ) for the ground state energies of the quantum LJAT trimers for several Z values.

Z	Ne_3	Ar_3	Kr_3	Xe_3
0.0	−1.506	−2.532	−2.754	−2.844
0.5	−1.231	−2.281	−2.507	−2.597
1.0	−0.970	−2.030	−2.260	−2.351
1.5	−0.704	−1.780	−2.013	−2.106

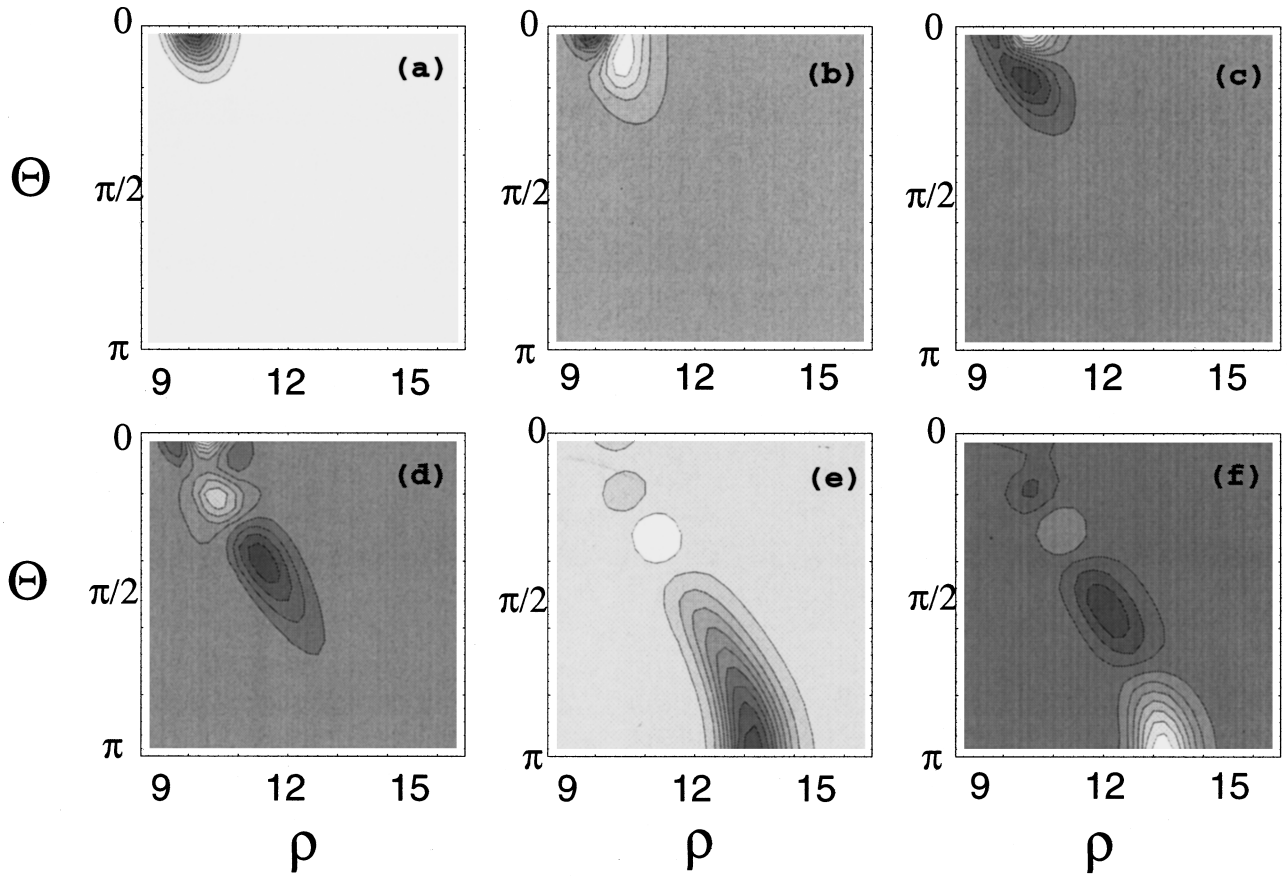

FIG. 7. Selected low-lying vibrational wave functions for the $Z=0.5$ Ar_3 trimer, shown as contour diagrams on the (θ,ρ) plane, which slices through the wave function at $\chi=0$. Panel (a) depicts the ground state $(n=0)$, and panels (b) through (f) show excited states $n=1$, 2, 5, 6, and 7 respectively.

ment between the two values becomes increasingly poor as Z increases.

One possible explanation for this behavior is that the normal mode approach (even when corrected for anharmonic vibrational effects [22]) underestimates the anharmonicity of the triangular minimum at higher Z values; based on an analogy with the diatomic Morse potential, this anharmonicity is expected to lower the energy of the vibrational ground state. Figure 1 shows that as Z increases and the energy of the triangular minimum increases, the basin surrounding this minimum becomes wider and increasingly anharmonic.

Previous studies of the LJ clusters showed that for particular vibrational states (or groups of states in narrow bands of energies), the probability density of the cluster's vibrational wave function was concentrated near the linear configuration [22]. The energy of the lowest state (or group of states) among these was therefore identified as the quantum mechanical equivalent of the classical transition state energy. For the LJAT trimers we also find vibrational states that are dominated by linear configurations; since the linear geometry is a local minimum on the PES for $Z\geqslant 0.4$, we anticipate that the tendency for the wave functions to peak near the linear configuration will be accentuated for Z values in this range.

Figures 7 and 8 show that this is indeed the case. Here we plot (in the APH coordinate system) several low-lying vibrational states for LJAT Ar_3 at $Z=0.5$ and $Z=1.5$; the plots are cuts through the three-dimensional wave functions at $\chi=0$. On these plots, $\theta=0$ corresponds to the equilateral triangle, while $\theta=\pi$ corresponds to the linear geometry. Figure 7(e) depicts the lowest-energy ''linear'' wave function of the $Z=0.5$ Ar_3 cluster, and Fig. 8(b) shows the lowest-energy ''linear'' state for the $Z=1.5$ Ar_3 cluster. It is clear that the wave function is more localized around the linear configuration at the higher value of Z, as expected. Note also that less vibrational excitation is required to reach the lowest-energy linear wave function at the higher Z value; for $Z=0.5$, the lowest linear state is the sixth excited state, while for $Z=1.5$ it is the first.

A similar graphical analysis of the vibrational states of all four trimers allows us to determine the energies of the lowest states, which may be described as linear. The energies of these states are listed in Table V. We see that in the Kr_3 and Xe_3 trimers much less vibrational excitation is required to reach the lowest-energy linear state at high Z values; the Ne_3 cluster, however, is not as sensitive to changes in Z, presumably because its low-lying wave functions are highly delocalized at all Z values. Graphical analysis of the Ne_3 eigenstates confirms this, and indicates that as Z increases, the ground state of the Ne_3 trimer becomes more delocalized across both the triangular and linear minima. This is in accord with the DQMC results shown in Fig. 6.

For the LJ clusters (where $Z=0$), it was found that the ratio between the energies of the vibrational ground state and the lowest ''linear'' wave function was always close to the value 0.677, which is the ratio between the classical potential

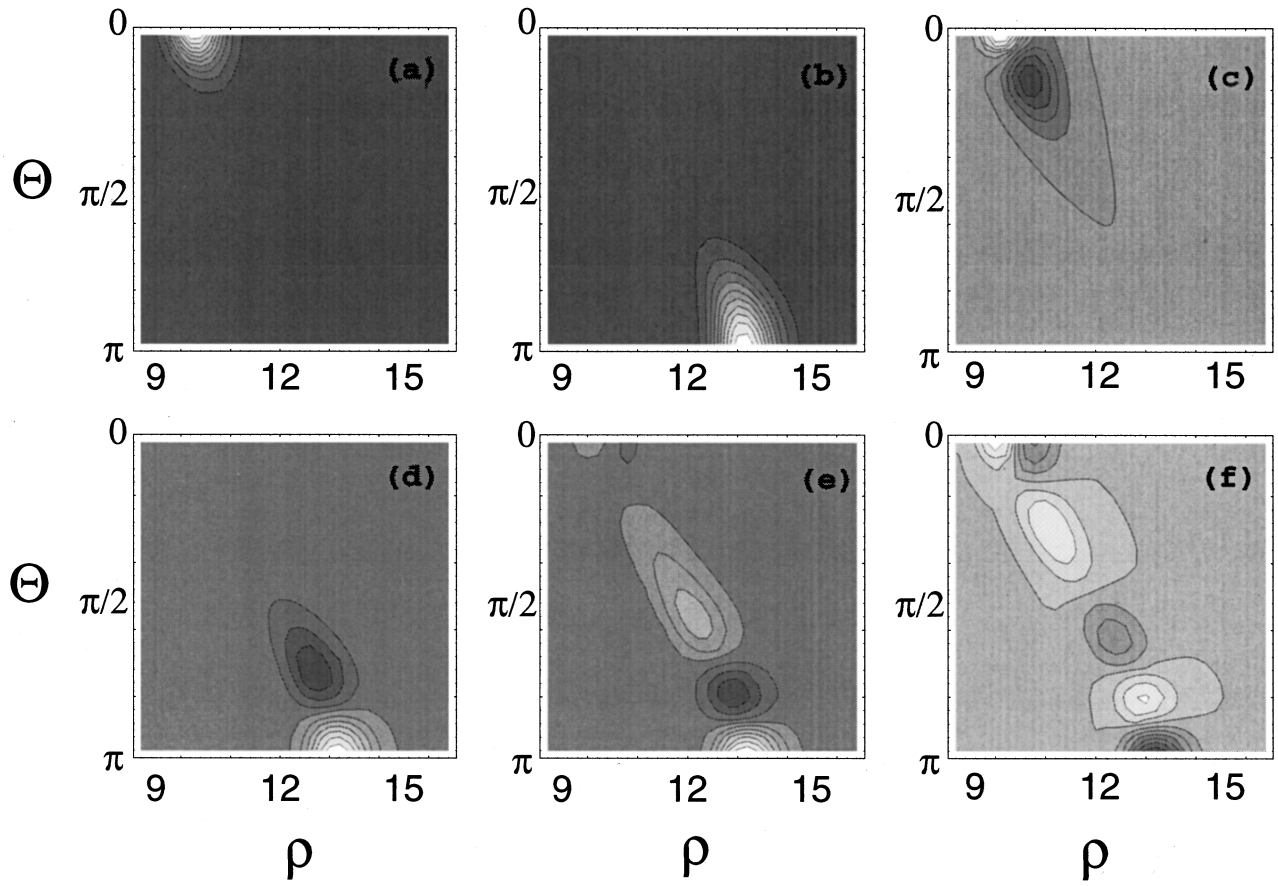

FIG. 8. The six lowest vibrational wave functions for the $Z=1.5$ Ar_3 trimer, shown as contour diagrams on the (θ,ρ) plane, which slices through the wave function at $\chi=0$. Panel (a) depicts the ground state ($n=0$), and panels (b) through (f) show excited states $n=1$ through $n=5$.

energies of the triangular and linear stationary points on the LJ PES. We have computed the ratios between the vibrational ground state and the lowest linear state for the four trimers and the three Z values we have examined; these ratios (along with the ratio of the classical energies) are listed in Table VI. We see that the energy ratios for the quantum LJAT clusters are typically quite close to their classically predicted values. The agreement is poorest for Ne_3, the cluster that shows the largest quantum effects; for the heavier clusters, the agreement between the quantum and classical ratios is best at small Z and worst at $Z=1.5$.

The linear geometry is a local minimum at the Z values we have studied; we can therefore once again use a normal mode approach to estimate the energies of the lowest linear wave function, and these estimates are listed in Table VII. The normal mode estimates are quite good at all of the Z values studied for the Ar_3, Kr_3, and Xe_3 clusters, but rather poor for the Ne_3 cluster. The relatively poor agreement between the normal mode model and the exact energies for Ne_3 is not too surprising given that this cluster deviates strongly from the classical picture at all Z values. For all four clusters, however, the normal mode estimates and exact quantum energies are in much better agreement for the linear configuration than for the triangular configuration.

TABLE V. Energies (in units of ϵ) of the lowest-energy ''linear'' wave functions of the quantum LJAT trimers for several Z values. The classical energy of the linear stationary point on the potential surface is given for comparison. The numbers in parentheses indicate the index of the vibrational state for each linear wave function, with $n=0$ being the ground state.

Z	Ne_3	Ar_3	Kr_3	Xe_3	Classical
0.0	−1.139	−1.731	−1.867	−1.923	−2.031
	($n=2$)	($n=10$)	($n=32$)	($n=79$)	
0.5	−1.187	−1.765	−1.910	−1.964	−2.075
	($n=1$)	($n=6$)	($n=18$)	($n=44$)	
1.0	−1.185	−1.794	−1.946	−2.007	−2.119
	($n=1$)	($n=3$)	($n=8$)	($n=19$)	
1.5	−1.194	−1.829	−1.986	−2.044	−2.164
	($n=1$)	($n=1$)	($n=3$)	($n=5$)	

TABLE VI. Ratios between the ground state energy and the energy of the lowest ''linear'' wave function of the quantum LJAT trimers at several Z values. The classical energy ratios are given for comparison.

Z	Ne_3	Ar_3	Kr_3	Xe_3	Classical
0.0	0.663	0.678	0.676	0.676	0.677
0.5	0.746	0.749	0.750	0.748	0.753
1.0	0.801	0.823	0.826	0.827	0.843
1.5	0.866	0.905	0.911	0.915	0.953

TABLE VII. Normal mode estimates (in units of ϵ) for the ''linear'' state energies of the quantum LJAT trimers for several Z values.

Z	Ne_3	Ar_3	Kr_3	Xe_3
0.0	−1.403	−1.718	−1.897	−1.926
0.5	−0.990	−1.731	−1.895	−1.960
1.0	−0.992	−1.762	−1.932	−1.999
1.5	−1.005	−1.796	−1.971	−2.040

We see from Figs. 7 and 8 that the low-lying vibrational states of both $Z=0.5$ and $Z=1.5$ Ar_3 are concentrated around the horseshoe orbit described previously. Similar results are obtained for the heavier trimers. The low-lying states in the Ar_3, Kr_3, and Xe_3 clusters all exhibit very regular and structured nodal patterns, as seen in these figures. These nodal patterns allow us to characterize the vibrational motion in these states, even if we cannot go so far as to assign quantum numbers to the eigenstates. For example, the second and third excited states shown in Fig. 8 for $Z=1.5$ Ar_3 are bending modes near the triangular and linear configurations, respectively. At higher energies (not shown here), we observe well-defined stretches localized near the linear configuration.

At even higher energies, though, the nodal patterns of the heavier trimers' eigenstates become increasingly irregular. Figure 9 depicts three vibrational states of $Z=1.5$ Xe_3 near the energy $E=-1.745\epsilon$. It is interesting to note that all three states remain concentrated along the horseshoe orbit despite their irregular nodal patterns. The finer details of the three wave functions, however, are different; the state in Fig. 9(a) is localized predominantly around the linear configuration, while that in Fig. 9(c) is mostly triangular. The intermediate state shown in Fig. 9(b) is spread along the horseshoe orbit, but appears to be mostly localized around the C_{2v} transition state.

We now turn to the question of whether the mixture of chaotic and regular classical dynamical behavior (Sec. IV) persists in the quantum clusters. To answer this question, we perform a statistical analysis of the vibrational energy spectrum of the Xe_3 cluster at $Z=1.5$. We choose to analyze the Xe_3 cluster because it has the highest level density of all of the trimers studied here, and is therefore most appropriate for an investigation of the spectral statistics. The large Z value was chosen to emphasize the effect of the three-body AT term on the vibrational spectrum. Recall that previous work has shown that the energy level statistics of the quantum LJ Ar_3, Kr_3, and Xe_3 clusters are close to those predicted by random matrix theory [22]; this finding is in accord with studies that suggest that the classical Ar_3 LJ cluster (which has $Z=0$) is largely chaotic at all but the lowest energies [14]. (However, we note that an analysis of large numbers of independent classical trajectories, like that presented in Sec. IV, was not done for the LJ Ar_3 cluster.)

We have obtained 273 converged energy levels for the $Z=1.5$ Xe_3 cluster in the range $-1.88\epsilon \leq E \leq -1.42\epsilon$; the distribution of energy level spacings and the spectral rigidity were computed for this stretch of energy levels, and the results are plotted in Fig. 10. We note that this range of ener-

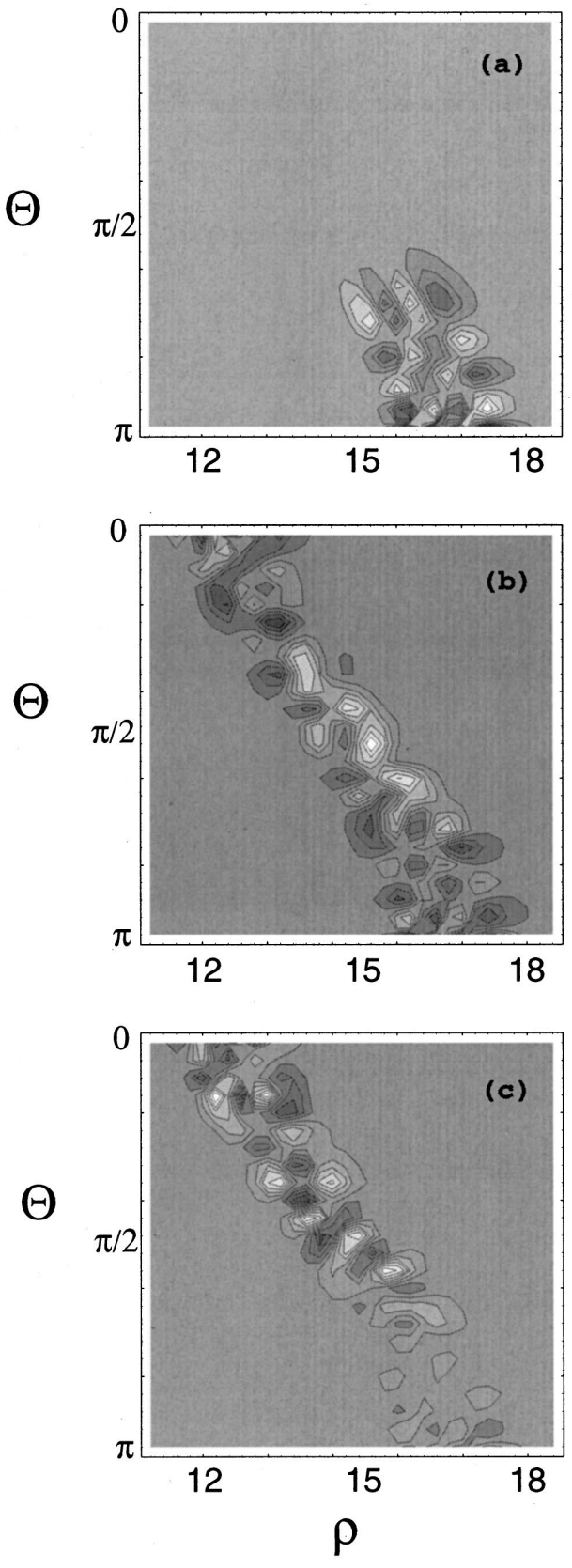

FIG. 9. Three highly excited vibrational wave functions for the $Z=1.5$ Xe_3 trimer, shown as contour diagrams on the (θ,ρ) plane, which slices through the wave function at $\chi=0$. Panel (a) shows the excited state $n=84$ at $E=-1.750\epsilon$; panel (b) shows the state $n=86$ at $E=-1.745\epsilon$; and panel (c) shows the state $n=87$ at $E=-1.742\epsilon$.

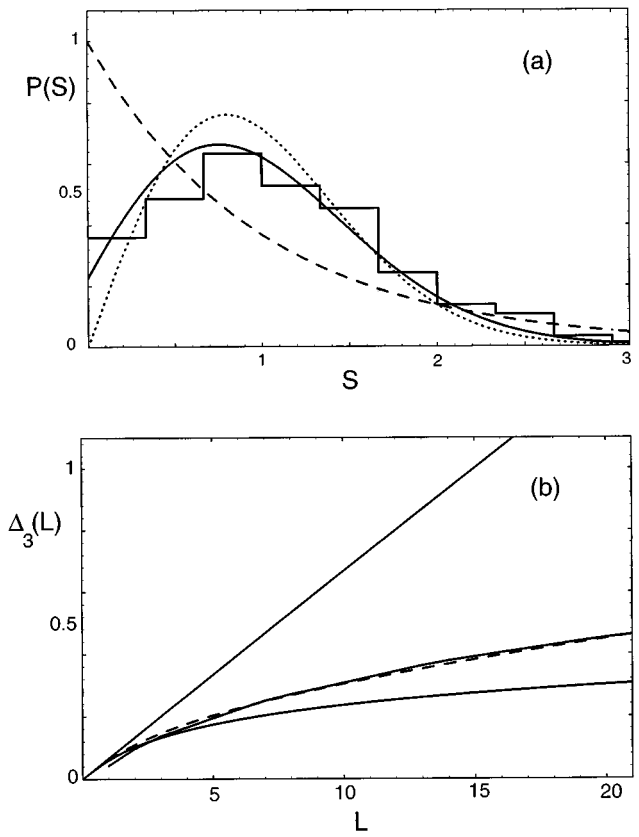

FIG. 10. (a) Distribution of nearest-neighbor energy level spacings for the 273 states in the energy range $-1.88\epsilon \leqslant E \leqslant -1.42\epsilon$ for the $Z=1.5$ Xe_3 trimer. The histogram represents the actual distribution of level spacings; the dotted and dashed curves are the Wigner and Poisson distributions respectively, and the solid curve is the Berry-Robnik prediction for $q=0.88$. (b) The spectral rigidity $\Delta_3(L)$ for the same set of levels as in (a). The middle solid curve is the result computed from the actual levels; the lower and upper solid curves are the random matrix and Poisson predictions, respectively. The dashed line is the Pandey interpolation with $q=0.88$.

gies is well above the classical transition state energy $E=-2.043\epsilon$ for $Z=1.5$.

Figure 10(a) shows the actual distribution of level spacings $P(S)$ and compares it to the Wigner and Poisson distributions. It is clear that the actual distribution is much closer to the Wigner distribution (obtained from random matrix theory), although the agreement is not perfect. To quantify the deviation of the actual $P(S)$ distribution from the Wigner limit, we have fitted the actual distribution to the Berry-Robnik interpolation formula, Eq. (7). The best agreement is obtained when the fraction of classical phase space occupied by chaotic trajectories is $q=0.88$. Figure 10(b) shows the spectral rigidity $\Delta_3(L)$ for the $Z=1.5$ Xe_3 cluster. Once again we find that the cluster lies between the RMT and Poisson limits, but closer to the RMT limit. The Pandey interpolation formula, Eq. (8), gives a good fit to the observed spectral rigidity when q is set to 0.88.

These results suggest that in the energy range $-1.88\epsilon \leqslant E \leqslant -1.42\epsilon$, the classical phase space of the Xe_3 trimer at $Z=1.5$ is predominantly chaotic, but also has a small regular component (about 12% of the total phase space volume). This picture is qualitatively similar to that deduced from the analysis of classical molecular dynamics trajectories in Sec. IV, and suggests that the quantum LJAT trimers incorporate the essential features of the mixed phase space picture developed there.

VI. CONCLUDING REMARKS: IMPLICATIONS OF MIXED PHASE SPACE

We find that the classical phase space of the LJAT trimers can be divided into three regions that are qualitatively different: one region is strongly chaotic, one is weakly chaotic, and one is quasiperiodic. This observation is characteristic of the phase space structure of a variety of few-degree-of-freedom conservative systems, in which the weakly chaotic region of phase space is associated with trajectories that exhibit intermittent dynamics. These intermittent trajectories spend long periods of time in the weakly chaotic region of phase space, punctuated by ''bursts'' of highly chaotic behavior as the trajectories flow into the strongly chaotic region of phase space.

This type of intermittent dynamical behavior has been the focus of a number of previous studies, both of low-dimensional Hamiltonian maps [41,48,49] and of the classical dynamics of the hydrogen atom in magnetic fields [50]. Sepúlveda *et al.* [51] identified a correspondence between the distribution of local Liapunov exponents and the power spectrum of classical trajectories that exhibit intermittency: quasiregular portions of a trajectory give rise to very small exponents that correlate closely with the sharp, narrow peaks of the power spectrum, while strongly chaotic portions of a trajectory yield larger local Liapunov exponents and correlate with the spectrum's broader features. The broad and narrow peaks that coexist in the power spectrum of intermittent trajectories in a model system were observed [51] to closely resemble those features found in power spectra of small molecular systems such as H_3^+ and Na_3. Presumably these molecular systems, like the LJAT trimers we have studied, exhibit dynamical intermittency.

How might this intermittency be reflected in the energy level spacing statistics of quantum mechanical LJAT trimers? In the semiclassical limit ($\hbar \to 0$), weakly chaotic phase space regions contribute ''irregular'' levels to the energy level spectrum, because classical trajectories passing through these regions are ultimately unstable. However, in the quantum mechanical clusters, the energy level spacing may be too large for such a weak instability to be reflected in the eigenstates.

Indeed, for the heaviest trimer in our study, Xe_3, the level spacing is on the order of 1 cm^{-1}, which is too large for the eigenstates to reflect the irregularity of a trajectory that spends about 1 ns undergoing essentially regular motion [52]. Thus for all of the quantum LJAT trimers studied here, the phase space region that we have characterized as weakly chaotic actually contributes *regular* dynamical character to the energy level spectrum. For example, the value of $q=0.88$ obtained for the Berry-Robnik level spacing parameter for $Z=1.5$ Xe_3 in the energy range $-1.88\epsilon \leqslant E \leqslant -1.42\epsilon$ can be interpreted to mean that at these energies, some 12% of the phase space is filled by *either* regular or weakly chaotic trajectories.

This conclusion is consistent with the classical results presented in Table II. This table shows that for energies above

$E=-1.65\epsilon$, the quasiperiodic portion of the classical phase space of $Z=1.5$ Xe_3 makes up less than 5% of the constant energy surface; another 10–15% of the phase space is occupied by the weakly chaotic region. Most of the quantum energy levels we have analyzed for $Z=1.5$ Xe_3 lie above $E=-1.65\epsilon$, and deviations from random matrix predictions for this system would therefore arise largely from states corresponding to weakly chaotic regions of phase space.

More subtle properties of the classical rare-gas trimers cannot be observed in their quantum counterparts without taking the trimers much farther towards the semiclassical limit. By tuning $\hbar$ to smaller values, we would be able to detect the influence of intermittent dynamical behavior in the quantum trimers. One effect would be to increase q to a value corresponding to the fraction of phase space that is either strongly or weakly chaotic. By varying $\hbar$ across a wide range of values, we could also study the influence of classical periodic orbits on the eigenstates of the quantum trimers, such as Taylor and co-workers [53] have recently done for HO_2.

Our study has revealed a number of similarities between the classical LJAT trimers and their quantum counterparts. The structures of minima and saddle points on the PES are revealed in the wave functions and the finite temperature properties of the quantum clusters. Both classical trajectory studies and an analysis of the energy level spacings of the quantum clusters show that the addition of the three-body AT term to the LJ pair potential creates a system whose phase space is mixed, with strongly chaotic, weakly chaotic, and quasiperiodic regions, over a large range of energies. Because the importance of the AT term can be controlled using the adjustable parameter Z, these LJAT clusters may be good model systems for further study of mixed phase space in classical and quantum mechanics.

ACKNOWLEDGMENTS

D.M.L. acknowledges support from the National Science Foundation via Grant No. CHE-9002637, awarded in 1991; R.J.H. acknowledges support from NSF Grant No. CHE-9203634, awarded in 1992. R.J.H. also thanks the Cambridge University Chemistry Department for the hospitality extended to him during a visit in October 1993. C.C. is grateful to Churchill College, Cambridge for financial support for the year 1993–1994. D.J.W. gratefully acknowledges financial support from the Royal Society of London.

[1] Faraday Disc. **97** (1994), special issue on structure and dynamics of Van der Waals complexes.
[2] Chem. Rev. **94**(7) (1994), special issue on Van der Waals molecules, edited by A. W. Castleman, Jr. and P. Hobza.
[3] V. R. Pandharipande, J. G. Zabolitzky, S. C. Pieper, R. B. Wiringa, and U. Helmbrecht, Phys. Rev. Lett. **50**, 1676 (1983).
[4] K. B. Whaley, Int. Rev. Phys. Chem. **13**, 41 (1994).
[5] S. Stringari and J. Treiner, J. Chem. Phys. **87**, 5021 (1987).
[6] T. R. Horn, R. B. Gerber, J. J. Valentini, and M. A. Ratner, J. Chem. Phys. **94**, 6728 (1991).
[7] D. J. Wales, J. Chem. Soc. Faraday Trans. **86**, 3505 (1990).
[8] H.-D. Meyer, J. Chem. Phys. **84**, 3147 (1986).
[9] Y. B. Pesin, Russ. Math. Surveys **32**, 55 (1977).
[10] Th. Zimmerman, L. S. Cederbaum, H.-D. Meyer, and H. Köppel, J. Phys. Chem. **91**, 4446 (1987).
[11] M. V. Berry and M. Robnik, J. Phys. A **17**, 2413 (1984).
[12] A. Pandey, Ann. Phys. (N.Y.) **119**, 170 (1979).
[13] D. J. Wales and R. S. Berry, J. Phys. B **24**, L351 (1991).
[14] R. J. Hinde, R. S. Berry, and D. J. Wales, J. Chem. Phys. **96**, 1376 (1992).
[15] G. Nyman, S. Nordholm, and H. W. Schranz, J. Chem. Phys. **93**, 6767 (1990).
[16] R. S. Dumont, J. Chem. Phys. **95**, 9172 (1991).
[17] Z. Bacić, R. M. Whitnell, D. Brown, and J. C. Light, Comput. Phys. Commun. **51**, 35 (1988).
[18] R. M. Whitnell and J. C. Light, J. Chem. Phys. **89**, 3674 (1988).
[19] R. M. Whitnell and J. C. Light, J. Chem. Phys. **90**, 1774 (1989).
[20] R. T Pack, Chem. Phys. Lett. **108**, 333 (1984).
[21] R. T Pack and G. A. Parker, J. Chem. Phys. **87**, 3888 (1984).
[22] D. M. Leitner, J. D. Doll, and R. M. Whitnell, J. Chem. Phys. **94**, 6644 (1991).
[23] J. B. Anderson, J. Chem. Phys. **63**, 1499 (1975).
[24] J. W. Negele and H. Orland, *Quantum Many-Particle Systems* (Addison-Wesley, New York, 1988).
[25] M. A. Suhm and R. O. Watts, Phys. Rep. **204**, 293 (1991).
[26] K. E. Schmidt and D. M. Ceperley, in *The Monte Carlo Method in Condensed Matter Physics*, edited by K. Binder (Springer, Berlin, 1992).
[27] B. L. Hammond, W. A. Lester, Jr., and P. J. Reynolds, *Monte Carlo Methods in Ab Initio Quantum Chemistry* (World Scientific, Singapore, 1994).
[28] J. D. Doll, D. L. Freeman, and T. L. Beck, Adv. Chem. Phys. **78**, 61 (1990).
[29] T. L. Beck, J. D. Doll, and D. L. Freeman, J. Chem. Phys. **90**, 5651 (1990).
[30] D. D. Frantz, D. L. Freeman, and J. D. Doll, J. Chem. Phys. **97**, 5713 (1992).
[31] C. Chakravarty, J. Chem. Phys. **99**, 8038 (1993).
[32] C. Chakravarty, J. Chem. Phys. **102**, 956 (1995).
[33] D. J. Wales, J. Chem. Soc. Faraday Trans. **88**, 653 (1992).
[34] D. J. Wales, J. Chem. Soc. Faraday Trans. **89**, 1305 (1993).
[35] D. J. Wales and J. P. K. Doye (unpublished).
[36] S. Wiggins, Physica D **44**, 471 (1990).
[37] R. E. Gillilan and G. S. Ezra, J. Chem. Phys. **94**, 2648 (1991).
[38] M. Berblinger, E. Pollak, and Ch. Schlier, J. Chem. Phys. **88**, 5643 (1988).
[39] J. M. Gomez Llorente and E. Pollak, J. Chem. Phys. **90**, 5406 (1989).
[40] O. Brass, J. Tennyson, and E. Pollak, J. Chem. Phys. **92**, 3377 (1990).
[41] Y. Kikuchi and Y. Aizawa, Prog. Theor. Phys. **84**, 563 (1990).
[42] E. Yurtsever and N. Elmacı, Phys. Rev. A **55**, 538 (1997).
[43] P. A. Braier, R. S. Berry, and D. J. Wales, J. Chem. Phys. **93**, 8745 (1990).

[44] R. J. Hinde, R. S. Berry, and D. J. Wales, J. Chem. Phys. **96**, 1376 (1992).
[45] R. J. Hinde and R. S. Berry, J. Chem. Phys. **99**, 2942 (1993).
[46] D. M. Leitner, R. S. Berry, and R. M. Whitnell, J. Chem. Phys. **91**, 3470 (1989).
[47] D. M. Leitner, J. D. Doll, and R. M. Whitnell, J. Chem. Phys. **96**, 9239 (1992).
[48] A. B. Zisook, Phys. Rev. A **25**, 2289 (1982).
[49] G. Stolovitzky and J. A. Hernando, Phys. Rev. A **43**, 2774 (1991).
[50] P. Schmelcher and L. S. Cederbaum, Phys. Rev. A **47**, 2634 (1993).
[51] M. A. Sepúlveda, R. Badii, and E. Pollak, Phys. Rev. Lett. **63**, 1226 (1989).
[52] Effects of time-scale separation of flow in classically chaotic systems on energy level statistics of the corresponding quantum mechanical system have been studied recently in other contexts. See O. Bohigas, S. Tomsovic, and D. Ullmo, Phys. Rep. **223**, 43 (1993); and D. M. Leitner, H. Köppel, and L. S. Cederbaum, Phys. Rev. Lett. **73**, 2970 (1994).
[53] H. S. Taylor (private communication).